

# Thermal relaxation of very small solar magnetic structures in intergranules: a process that produces kG magnetic field strengths

J. Sánchez Almeida

*Instituto de Astrofísica de Canarias  
E-38200 La Laguna, Tenerife, Spain*

jos@ll.iac.es

## ABSTRACT

The equilibrium configuration of very small magnetic fluxtubes in an intergranular environment automatically produces kG magnetic field strengths. We argue that such process takes place in the Sun and complements the convective collapse (CC), which is traditionally invoked to explain the formation of kG magnetic concentrations in the solar photosphere. In particular, it can concentrate the very weak magnetic fluxes revealed by the new IR spectro-polarimeters, for which the operation of the CC may have difficulty. As part of the argument, we show the existence of solar magnetic features of very weak fluxes yet concentrated magnetic fields (some  $3 \times 10^{16}$  Mx and 1500 G).

*Subject headings:* Magnetic fields — MHD — Sun: faculae, plages — Sun: granulation — Sun: magnetic fields — Sun: photosphere

## 1. Introduction and rationale

Except for sunspots and pores, the solar magnetic features are not spatially resolved. These unresolved structures tend to have highly concentrated kG magnetic fields, a fact which was already acknowledged by the early seventies (Beckers & Schöter 1968; Harvey et al. 1972; Stenflo 1973; Wiehr 1978). Although such extreme concentration of the fields was never anticipated from basic physical principles, a mechanism that explains them came up soon after the discovery. The so-called Convective Collapse (hereafter CC; Parker 1978; Spruit 1979) is a modification of the convective instability that drives the transport of energy in the envelopes of cool stars. The hydrostatic equilibrium stratification is unstable against vertical displacements, a factor that amplifies adiabatic vertical motions (e.g., Cox & Giuli 1968). The same phenomenon takes place in magnetized plasmas and favors down-drafts

along vertical field lines. These down-drafts evacuate the magnetic structures which seek a new stable equilibrium by increasing the magnetic field strength. (For details on the CC see, e.g., Parker 1979; Spruit 1981.) Although there is no conclusive observation proving that the CC causes the formation of the intense photospheric fields, it is systematically invoked to explain them.

As any other process to concentrate magnetic fields, the CC does not modify the magnetic flux of the region whose field strength is being increased. Precursor regions having large magnetic flux are required to yield regions of concentrated magnetic fields with large flux. However, the observations show an embarrassing lack of precursors having the fluxes of typical network magnetic concentrations<sup>1</sup>, i.e., between  $10^{17}$  Mx and  $10^{18}$ Mx (see Fig. 1). One may attribute the absence of precursors to the speed of the CC process, so that the chances of detecting a feature in its pre-collapse phase are negligible. This argument is difficult to maintain since the growth time of the CC instability is at least several minutes (e.g., Hasan 1986; Takeuchi 1999; Rajaguru & Hasan 1999), which represents a sizeable fraction of the observed lifetimes of the magnetic concentrations (some 10-20 minutes, e.g., Muller 1994; Berger & Title 1996). This shortage of large flux but weak field strength features suggests that the concentration of quiet Sun magnetic fields proceeds in a hierarchical way, starting from the reservoir of unstable weak flux regions that are indeed observed (see the lower left corner in Fig. 1). These weak fluxes are first amplified to kG field strengths and the subsequent coalescence of many features renders structures with the observed flux. The concentration of weak fluxes poses a problem to the CC, though. Weak fluxes correspond to small structures for which the radiative exchange of heat with the surroundings is very efficient, hampering an adiabatic evolution of the magnetized plasma. This heat leakage frustrates the full development of the CC instability (e.g., Venkatakrisnan 1986; Hasan 1986; Schüssler 1986). Despite the fact that the observed weak field features are still liable for the CC (Fig. 1), it would be desirable having an alternative physical mechanism that is efficient even for limited magnetic fluxes. The purpose of the paper is to point out that such a mechanism emerges in a natural way from the numerical simulations of the solar granulation: the equilibrium configuration of a km-wide flux concentration standing in an intergranular environment automatically produces kG field strengths. For lack of a better term it will be denoted as TRIP, an acronym for Thermal Relaxation within Intergranule Process. A detailed theoretical study of the mechanism goes beyond the scope of the paper. We just point out that it can operate in the Sun, which opens up new possibilities to be explored elsewhere, both by numerical experiments and from an observational point of view.

---

<sup>1</sup>The limit set by Howard & Stenflo (1972) that at least 90% of the flux observed in the traditional magnetograms is in the strong field regime expresses the same idea.

Some of the possibilities are gathered in §5.

## 2. Physical scenario

Intense quiet Sun magnetic concentrations<sup>2</sup> are found in the intergranular lanes (Sheeley 1967; Dunn & Zirker 1973; Mehlretter 1974; Muller 1985). The intergranules are cooler than the mean photosphere, yet maintain a high pressure. This extra pressure arises to slow down the horizontal motions of the plasma that, eventually, sinks back to the sub-photosphere following intergranular down-drafts. As it is described by Stein & Nordlund (1998), the convergence of the flows towards the intergranular lanes is responsible for an augment of dynamic pressure that balances the deficit of temperature. First, outflows from adjacent granules collide at the intergranular lanes. Second, the shear of these colliding flows produces whirls which generate turbulent motions and therefore turbulent pressure. .

Assume for the moment that the magnetic structures live long enough to reach both, thermal equilibrium with the surroundings, and mechanical equilibrium within their intergranular environment. We will see that this configuration automatically demands a strong concentration of the magnetic fields with increasing height in the atmosphere. Let us condense the equations that describe the equilibrium. They can be found elsewhere (e.g. Parker 1979; Chapter 8), but we list them here to introduce the notation. Assume vertical fluxtubes embedded in an intergranular environment. The mechanical equilibrium requires that the gas pressure within the concentration  $P$ , plus the magnetic pressure due to the magnetic field strength  $B$ , balance the mean external pressure  $P_e$ . This balance occurs at every height in the atmosphere  $z$ ,

$$P_e(z) = P(z) + B^2(z)/(8\pi). \quad (1)$$

Together with this mechanical balance across field lines, there should be hydrostatic equilibrium along field lines where Lorentz forces play no role. Then the drop of pressure from a reference height  $z_0$  follows an exponential law,

$$\ln[P(z)/P(z_0)] = - \int_{z_0}^z H(z')^{-1} dz'. \quad (2)$$

The pressure scale height  $H(z)$  is roughly proportional to the temperature. Combining equation (1) with the definition

$$B_m^2(z) = 8\pi P_e(z), \quad (3)$$

---

<sup>2</sup>The term *quiet Sun magnetic fields* is used throughout the text in a broad sense, implying everything but sunspots and pores.

one ends up with

$$[B(z)/B_m(z)]^2 = 1 - \{1 - [B(z_0)/B_m(z_0)]^2\} \{[P(z)/P(z_0)]/[P_e(z)/P_e(z_0)]\}, \quad (4)$$

where  $B_m(z)$  represents for the maximum possible field strength at every height. The fact that the temperature of the intergranule is smaller than that of the mean photosphere implies that  $H < H_e$ , where  $H_e$  is the pressure scale height ascribed to a  $P_e$  that also satisfies equation (2). Since  $H < H_e$ ,  $P$  drops with height faster than  $P_e$  (eq. [2]). No matter the initial magnetic field strength, equation (4) predicts

$$B(z)/B_m(z) \sim 1 \text{ when } z \gg z_0. \quad (5)$$

The magnetic field strength always tend to reach its maximum possible value set by the external gas pressure.

Is this mechanism of relevance for the concentration of quiet Sun magnetic fields? One can advance a positive answer to the question using the analytic expressions corresponding to isothermal atmospheres. Under this hypothesis  $H$  and  $H_e$  are constant, therefore,

$$\ln[P(z)/P(z_0)] = -(z - z_0)/H, \quad (6)$$

$$\ln[P_e(z)/P_e(z_0)] = -(z - z_0)H_e,$$

which transform equation (4) into

$$[B(z)/B_m(z)]^2 = 1 - \{1 - [B(z_0)/B_m(z_0)]^2\} \exp[-(z - z_0)/\langle H \rangle], \quad (7)$$

$$\langle H \rangle = HH_e/(H_e - H).$$

Considering that deep down in the atmosphere the magnetic fields are not dynamically important ( $B[z_0]/B_m[z_0] \ll 1$ ), the solution (7) becomes independent of  $B(z_0)$ ,

$$[B(z)/B_m(z)]^2 = 1 - \exp[-(z - z_0)/\langle H \rangle]. \quad (8)$$

The scale height  $\langle H \rangle$  turns out to be about 225 km, a figure which comes out from the pressure scale height  $H_e \sim 150$  km and intergranular lanes 40% cooler than the mean photosphere ( $H/H_e \sim$  temperature intergranule/mean temperature  $\sim 0.6$ ). The values for  $B/B_m$  observed in the photosphere (some 0.9; e.g. Rüedi et al. 1992; Sánchez Almeida & Lites 2000) are reached if the imbalance of temperatures extends for at least 400 km, which is sound according to the numerical simulations of solar granulation (see, Stein & Nordlund 1998, and the forthcoming §2.1). In short, magnetic concentrations in equilibrium in an intergranule automatically demand kG fields at photospheric levels.

## 2.1. More realistic estimate

The order of magnitude estimate described above has been refined using realistic model atmospheres from the numerical simulations of solar granulation by Stein & Nordlund (1998). Figure 2, left, shows the temperatures of two intergranules and the mean temperature of the atmosphere. Figure 2, right, includes the mean pressure of the atmosphere, as well as the gas pressure to be expected if the intergranules were in hydrostatic equilibrium. The hydrostatic equilibrium pressures were computed from the temperatures by integration of equation (2) with  $z_0 = -1.5$  Mm. First note the large deficit of hydrostatic equilibrium pressure with respect to the mean pressure. Since the total pressure within intergranules has to be high (refer to §2), the mean pressure of the atmosphere is a reasonable guess to describe  $P_e(z)$ . Consequently, there is a large difference between  $P_e$  and  $P$  which a magnetic structure will tend to balance by increasing the magnetic pressure<sup>3</sup>. Figure 3 shows the magnetic field strengths that guarantee mechanical equilibrium within the two intergranular environments. We have just employed equations (3) and (4), combined with the pressures in Figure 2. The resulting field strengths are well within kG regime at the base of the photosphere ( $z = 0$ ). Figure 3 includes  $B/B_m$ , which turns out to be about 0.9 in the photosphere. This figure is also in good agreement with observations (Rüedi et al. 1992; Sánchez Almeida & Lites 2000). We have not mentioned the magnetic field strength at the bottom of the atmosphere  $B(z_0)$  since it does not affect the final field strength; see appendix A. The intergranular temperature is more important to produce kG fields. However, appendix A points out that a 1200 K temperature change modifies the final field strength by only 10%.

van Ballegoijen (1984), and later Hassan & van Ballegoijen (1998), investigated the field strength of magnetic concentrations trapped in intergranules that are not in hydrostatic equilibrium. Specifically, they consider the modifications of pressure due to the vertical gradient of the vertical convective velocity. Magnetic field strengths of the order of  $B(0)/B_m(0) \sim 0.6$  balance the extra pressure that arises (Hassan & van Ballegoijen 1998). Although these field strengths are smaller than the values that we get, they already indicate that kG are needed to compensate deviations from hydrostatic equilibrium in intergranules.

---

<sup>3</sup>Incidentally, this imbalance between the hydrostatic equilibrium pressure and the effective pressure is responsible for the negative buoyancy forces that drive the down-drafts in the intergranular lanes.

### 3. Time scales to reach equilibrium

The arguments in the previous section rely on a magnetic concentration which has reached equilibrium within an intergranule. Here we aim at showing whether the assumption is reasonable or, more precisely, at investigating the conditions that make it reasonable. We compare the observed life times of solar structures with the time scales of various physical processes required to achieve equilibrium: the time to reach the temperature stratification of the environment, the time to set hydrostatic equilibrium along field lines, the ohmic diffusion time scale, the viscous time scale, and the ambipolar diffusion relaxation time scale.

*Thermal relaxation time scale*, or the time scale to cool down to intergranular temperatures. We neglect the convective transport so that the transfer of heat is solely carried by radiation<sup>4</sup>. The time to attain the temperature of the environment is approximately given by the radiative relaxation time  $t_{th}$ ,

$$t_{th} = \frac{C_V}{16\kappa_R\sigma T^3} [1 - \tau \arctan(1/\tau)]^{-1}, \quad (9)$$

$$\tau = \kappa_R \rho a, \quad (10)$$

where the new symbols stand for the Stefan-Boltzmann constant  $\sigma$ , the Rosseland mean absorption coefficient  $\kappa_R$ , the specific heat at constant volume  $C_V$ , and the density  $\rho$  (Spiegel 1957; Hasan 1986; Stix 1991). The time  $t_{th}$  depends on the horizontal thickness of the magnetic concentration, which is parameterized in equation (10) as the radius of the tube  $a$ . Let us denote by  $r(z)$  the radius of a fluxtube in equilibrium within an intergranule; it varies with height to satisfy the conservation of magnetic flux  $\Phi$ ,

$$\Phi = \pi r^2(0)B(0) = \pi r^2(z)B(z). \quad (11)$$

Assume that this fluxtube was initially in hydrostatic equilibrium with the mean photosphere. We try to evaluate the relaxation time for this structure to reach the intergranular temperature. The initial magnetic field strength is therefore given by equations (2) and (4) with  $H(z) = H_e(z)$ ,

$$B_i(z) = B_i(0)B_m(z)/B_m(0). \quad (12)$$

The evolution from the initial values  $B_i$ ,  $r_i$  to  $B$ ,  $r$  conserves the magnetic flux, i.e.,  $\Phi$  is also  $\pi r_i^2 B_i$ . Using equations (11) and (12), the radius required to evaluate  $t_{th}$  can be given as a function of the magnetic flux  $\Phi$  and the initial field at the base of the photosphere  $B_i(0)$ ,

$$r_i(z) = \left[ \frac{\Phi B_m(0)}{\pi B_i(0) B_m(z)} \right]^{1/2}. \quad (13)$$

---

<sup>4</sup>Convection speeds up the heat transfer, therefore, the real relaxation times will be even shorter than the ones estimated here.

Figure 4 shows  $t_{th}$  for a fluxtube with the radius given by equation (13) and embedded in the coolest model intergranule of Figure 2. (No significant difference is found when employing the other intergranule.) The Rosseland mean opacity required to evaluate  $t_{th}$  was obtained from Seaton et al. (1994), whereas the specific heat has been computed following Mihalas (1967). Figure 4 shows the cooling time for a structure having  $\Phi \simeq 5 \times 10^{13}$  Mx and  $B_i(0) = 200$  G, which will finish with a radius  $r(0) = 1$  km. The effective time scale is set by largest cooling time within the 400 km region below the photosphere (where the TRIP operates; see §2). This particular structure cools down in a tenth of a minute, therefore, it easily reaches the temperature of the intergranular environment. As structures of larger sizes are considered, the cooling time increases. The dependence can be worked out taking into account that the largest cooling time occurs at the bottom of the region of interest, where the fluxtube is optically thick. In this case  $t_{th}$  scales with the square of the radius (e.g., Stix 1991), that is to say, with  $\Phi/B_i(0)$  (eq.[13]). With the multiplying constant obtained from Figure 4 at  $z = -400$  km, one finds that

$$t_{th} \simeq 15 \text{ min } [\Phi/1.2 \times 10^{17} \text{ Mx}] [B_i(0)/1800 \text{ G}]^{-1}. \quad (14)$$

For the cooling to be effective,  $t_{th}$  has to be shorter than the observed lifetimes (some 15 min, e.g., Muller 1994; Berger & Title 1996). The condition  $t_{th} < 15$  min and equation (14) render

$$\Phi < 1.2 \times 10^{17} \text{ Mx } [B_i(0)/1800 \text{ G}], \quad (15)$$

or, using equation (11) with  $B(0)$  given by the model intergranule,

$$r(0) < 49 \text{ km } [B_i(0)/1800 \text{ G}]^{1/2}. \quad (16)$$

Taking into account that  $B_i(0) < B_m(0) \sim 1800$  G, the two equations (15) and (16) set absolute upper limits to the magnetic flux and size that can be concentrated, explicitly,  $\Phi < 1.2 \times 10^{17}$  Mx, and  $r(0) < 49$  km. For structures well below the kG regime, say  $B_i(0) \leq 500$  G, the limits are tighter,

$$\Phi < 3.3 \times 10^{16} \text{ Mx}, \quad (17)$$

$$r(0) < 26 \text{ km}. \quad (18)$$

*Time scale to reach mechanical equilibrium.* Think of a precursor fluxtube in hydrostatic equilibrium having the mean photospheric temperature. It is now moved to an intergranular space so that it rapidly cools down to the new temperature. This intermediate structure is no longer in equilibrium and requires a time to adjust pressure and magnetic field according to the new situation. This time scale,  $t_{he}$ , is the one that we try to estimate. The new equilibrium will be set within the time required for pressure and magnetic field perturbations

to propagate throughout the structure. Given a characteristic propagation speed  $U$ ,  $t_{he}$  scales with the extent of the region  $l$ , namely,

$$t_{he} \sim l/U. \quad (19)$$

Since we deal with thin structures, the overall time scale will be set by the length of the structure rather than the radius. The speed  $U$  can be estimated as the propagation speed of magneto-acoustic waves in magnetic fluxtubes. Different magneto-acoustic modes are characterized by different velocities, but there is always a plane wave mode which propagates at the sound speed of the external medium (see Spruit 1982 and references therein). The speeds of other modes are combinations of Alfvén speeds and sound speeds. When the magnetic field strength is weak, Alfvén speeds are smaller than the sound speeds and the fastest mode travels at the sound speed. On the contrary, strong field implies modes faster than the sound speed. Consequently,  $U \leq c$ ,  $c$  being the sound speed of the external medium. An estimate of the time to reach hydrostatic equilibrium results  $t_{he} \sim l/c$ , with  $l \sim 400$  km, i.e., the range of heights producing the increase of field strength (see §2).  $t_{he}$  is represented in Figure 4, where the adiabatic exponent required to evaluate  $c$  has been computed according to Mihalas (1967). The largest time scale within the 400 km below the photosphere is about one minute. This time interval is reasonable and similar (although shorter) than the time needed for the CC to operate (Hasan 1986; Takeuchi 1999; Rajaguru & Hasan 1999). In any case, the fluxtubes have enough time to reach hydrostatic equilibrium during their lifetimes.

*Magnetic diffusion time scale.* Since we are dealing with very narrow structures (see eqs. [16] and [18]), they quickly diffuse away in a plasma with finite electrical conductivity. Should this diffusion be fast enough, it may frustrate the concentration process. The induction equation predicts the smear of magnetic structures in a diffusion time scale  $t_{md}$ . It is set by the square of the characteristic length scale over the magnetic diffusivity  $\eta$  (e.g., Parker 1979). Using  $\eta \sim 10^9$  cm<sup>2</sup> s<sup>-1</sup> and the radius in equation (13), the fluxtube in Figure 4 has  $t_{md} \gg t_{th}$ . Since the scaling with the tube radius is the same for both  $t_{md}$  and  $t_{th}$ , the fact that  $t_{md} \gg t_{th}$  holds independently of the tube size. In short, the magnetic diffusion cannot counteract the thermal relaxation. On the other hand, ohmic diffusion may frustrate the concentration if it becomes faster than the time to reach hydrostatic equilibrium. The process requires  $t_{md} \simeq r_i^2(z)/\eta > t_{he}$ . This inequality sets a lower bound to the sizes and fluxes that can be concentrated, namely,

$$r(0) > 3 \text{ km } [B_i(0)/1800 \text{ G}]^{1/2}, \quad (20)$$

$$\Phi > 4 \times 10^{14} \text{ Mx } [B_i(0)/1800 \text{ G}]. \quad (21)$$

The limits were deduced from the fluxtube in Figure 4, that borders on  $t_{md} = t_{he}$  at  $z = -0.5$  Mm. Two comments on the magnetic diffusivity that we have used to estimate  $t_{md}$  are in

order. First, the figure  $10^9 \text{ cm}^2 \text{ s}^{-1}$  represents the maximum value at photospheric levels and, consequently, an upper limit for the diffusivity in the layers of interest (Kovitya & Cram 1983). Second, we consider ohmic diffusion, but we may as well employ turbulent diffusion. Both diffusivities are similar for the range of very narrow fluxtubes that we study (see Schüssler 1986).

*Viscous time scale.* The concentration of magnetic fields require the motions within the fluxtubes to be spatially disconnected from the motions of the external non-magnetic medium. This horizontal gradient of velocity represents a large shear that may be impeded by viscous stresses. The time scale for viscous stresses to operate,  $t_{vs}$ , is formally identical to the magnetic diffusion time scale, except that the diffusivity  $\eta$  has to be replaced with the kinematic viscosity  $\nu$ . Since  $\nu \ll \eta$  (Kovitya & Cram 1983),  $t_{vs} > t_{md}$  and viscosity does not hamper the concentration process. One can also consider turbulent viscosity without changing this conclusion since it is similar to the magnetic diffusivity (Schüssler 1986).

*Ambipolar diffusion time scale.* If collisions between ions and neutrals are not frequent, the neutrals are allowed to drift across field lines. In our case, driven by the gradient of gas pressure between the external medium and the fluxtube, this ambipolar diffusion produces a flow of neutrals tending to fill up the magnetic concentration (Giovanelli 1977). The characteristic time for ambipolar diffusion to operate is,

$$t_{ad} \sim r_i(z)/u_d, \quad (22)$$

with  $u_d$  the velocity of the drift (e.g., Parker 1963; Giovanelli 1977). According to Parker (1979; §4.6),

$$u_d \simeq 0.4 \text{ cm s}^{-1} \left[ \frac{r_i(z)}{1 \text{ km}} \right]^{-1} \left[ \frac{B(z)}{1500 \text{ G}} \right]^2 \left[ \frac{n(z)}{10^{17} \text{ cm}^{-3}} \right]^{-2} \left[ \frac{\chi(z)}{10^{-2}} \right]^{-1}, \quad (23)$$

where the symbols  $\chi$  and  $n$  stand for the degree of ionization and the number of neutrals per unit volume, respectively. According to equation (23), ambipolar diffusion becomes important in low density weakly ionized media, properties that do not characterize the sub-photosphere where the TRIP takes place. The normalization factors for  $\chi$ ,  $n$  and  $B$  in equation (23) correspond to the typical values in the sub-photospheric layers (e.g., Stein & Nordlund 1998, and Fig. 3). Under these conditions, the tiny drifts predicted by equation (23) imply time scales of days even for the smallest fluxtubes considered here. For example,

$$t_{ad} \simeq 3 \text{ days}, \quad (24)$$

when  $r_i(z) = 1 \text{ km}$ . Since the TRIP occurs in minutes (Fig. 4), ambipolar diffusion cannot impede it.

According to the estimates carried out in the preceding paragraphs, the TRIP operates as soon as the magnetic flux is within the bounds set by equations (15) and (21). Then the process is not damped by ohmic diffusion, and it evolves faster than the observed life time of the magnetic concentrations. Under such conditions, the equilibrium demands kG magnetic field strengths at photospheric levels.

#### 4. Detection of weak flux yet concentrated magnetic fields

As part of the discussion on the interest of the work (§1), we argued that the seemingly empty upper left corner in Figure 1 is actually filled. It corresponds to magnetic fields which could have been concentrated by the TRIP and whose weak flux precursors are observed (the data in the lower left corner of the same figure). We pointed out that the sensitivity of the current measurement hinders the detection. To support this claim, the point represented by the black spot with error bars was added to Figure 1. It stands for a feature with  $B(0) \simeq 1450$  G and  $\Phi \simeq 2.8 \times 10^{16}$  Mx, whose properties have been deduced from polarized spectra in the limit of sensitivity of the present solar polarimeters. This section aims at explaining how the existence of this weak flux but concentrated field was deduced, which illustrates the observational difficulties to sample the region of interest.

The point comes from the same data leading to the shadowed region in Figure 1 (Sánchez Almeida & Lites 2000). Since we seek fluxes weaker than the weakest analyzed in the previous work, the portion of the solar surface discarded in the original analysis is used here. In particular, we selected those pixels with polarization signals of the order of the noise of the individual spectra (below  $10^{-3}$ , in units of the continuum intensity). The corresponding Stokes  $V$  profiles<sup>5</sup> of the Fe I lines at 6301.5 Å and 6302.5 Å were classified with a cluster analysis algorithm (see Sánchez Almeida & Lites 2000 for details). The resulting mean profiles corresponding to different classes were visually inspected for Stokes  $V$  signals with the characteristic shape of strong fields (i.e., with the classical shape observed in plage regions; Baur et al. 1981; Stenflo et al. 1984). Note that the noise of these mean profiles is greatly reduced by the averaging of several hundred individual profiles, so that extremely weak polarization signals are now detectable. Several mean profiles with the right shape were reproduced using the inversion code by Sánchez Almeida (1997) which, among other physical parameters, assigns magnetic field strengths. The example used to set the point in Figure 1 is shown in Figure 5. The figure includes a magnetogram of the region pointing out

---

<sup>5</sup>The term Stokes  $V$  profile denotes the variation with wavelength of the degree of circular polarization. It corresponds to the customary representation of the line polarization used to measure solar magnetic fields.

the pixels from which mean profile was constructed. This inset proves that our mean profile is not an instrumental artifact produced by leakage of network polarization (note that the selected points bear no obvious spatial coincidence with the network). The observed Stokes  $I$  and  $V$  profiles as well as the synthetic counterparts used to infer the physical properties are in Figure 5. In addition, we include best fitting synthetic profiles deduced by the inversion code when the magnetic field strength at  $z=0$  is forced to be some 500 G. Obviously the fit worsens or, in other words, despite the weakness of the flux, our data correspond to regions having field strengths well above 500 G. The error bar of the magnetic field strength in Figure 1 corresponds to the standard of error of the non-linear  $\chi^2$ -minimization algorithm used to carry out the fits (e.g., Bevington 1969). The error of the flux is just the difference of flux between the two fits in Figure 5.

The Stokes  $V$  spectra from which the magnetic field was deduced have an extremely small noise (some  $10^{-4}$  in units of the continuum intensity). Improving this level represents a challenge, but it mandatory to sample the (still) empty region in the upper left corner of Figure 1. Note that using the highly split near IR lines from which the weak fluxes in Figure 1 were deduced does not help. For reasons explained in Sánchez Almeida & Lites (2000), the IR lines are good for weak field strengths but their signals weaken for strong fields. For example, the synthesis of Fe I  $\lambda 15648$  in the model atmosphere that reproduces the polarization in Figure 5 yields a peak polarization 4 times weaker than that observed with Fe I  $\lambda 6302.5$ . The region would be undetectable if observed in the IR.

In addition to the limited sensitivity of the current polarimeters, there are basic conceptual difficulties to interpret the polarization observed at these weak fluxes: extreme line asymmetries, mixed polarities within the resolution elements, etc. These problems are discussed elsewhere (e.g., Sánchez Almeida 1998), but one have to keep in mind that they also handicap precise determinations of field strength and flux.

## 5. Discussion and conclusions

Structures having weak magnetic fluxes ( $\leq 3 \times 10^{16}$  Mx) and standing in an intergranular environment develop kG field strengths in a few minutes. We argue that this concentrated state represents the equilibrium configuration of such structures and their natural endpoint. This new mechanism for magnetic field concentration complements the traditional Convective Collapse (CC) in the sense that it works for very weak fluxes, a factor that hinders the CC. However, the mechanism is reminiscent of the CC in many respects. In both cases the temperature of the magnetic concentration becomes smaller than the one required to balance the pressure stratification of the environment. The difference has to do with the physical

effect responsible for this temperature deficit. In the case of the CC, it is produced by adiabatic displacements of plasma blobs in a superadiabatic temperature stratification. In the TRIP (Thermal Relaxation within Intergranule Process), it is produced by the radiative cooling to reach the temperatures of the high pressure but cool intergranular environment. These special physical conditions that trigger the TRIP automatically appear in the numerical simulations of solar granulation (Stein & Nordlund 1998, and references therein). The motions towards and within intergranules yield the surplus of dynamic pressure (§2). On the other hand, the global pattern of the convective motions provides another key ingredient of the process. As we pointed out in the introduction, the formation of typical network magnetic concentrations ( $10^{17}$ – $10^{18}$  Mx) requires gathering many TRIP fluxtubes. This step of the process has to be hypothesized since a direct observation remains beyond our technical capabilities (see §4). The granular motions offer a gathering mechanism. They tend to drag all magnetic concentrations towards the vertices where several intergranules meet, thus inducing the formation of conglomerates of magnetic structures (e.g., Cattaneo 1999). The hypothesis of formation by coalescence has an independent observational support. It is observed among the smallest magnetic structures presently detected. The so-called G-band bright points, which we believe to trace magnetic concentrations, continuously split and merge, changing shape, and presumably magnetic flux, in less than a minute (Berger & Title 1996). Moreover, they are swept towards the vertices by the granular flow (e.g. Berger & Title 1996; van Ballegoijen et al. 1998). The extrapolation of such observed behavior to our much smaller elements results very reasonable. In particular, because the importance of the drag force that couple the fluxtube motions to the granular flows augments as the structure becomes thinner (e.g., Meyer et al. 1979; Schüssler 1986). Two additional features of the granular flow may also be relevant for the concentration process. First, the continuous advection of fresh magnetized plasma replenishes that part of the concentrations lost by ohmic diffusion, sucked by the down-drafts, etc. Second, the rather common intergranular whirls provide stabilizing effects upon the magnetic concentrations that get caught within them (Schüssler 1986).

A sign that the TRIP operates in the Sun would be finding a population of solar magnetic structures having 1.5 kG field strength and  $10^{16}$  Mx (radius of some 14 km). Although it still functions, the CC tends to produce field strengths of 1 kG rather than 1.5 kG (e.g., Takeuchi 1999). Such difference offers a real chance for distinguishing the outcomes of the two processes. These hypothetical features should occupy the empty upper left corner of Figure 1, where exploration with the present means is full of technical difficulties (see §4). Fortunately, they may be detected pushing the current instruments to their limits, therefore, devoted observations are possible and eagerly awaited.

We have offered order of magnitude arguments to support the TRIP. They have to be

corroborated by numerical simulations showing the formation of kG magnetic structures in intergranules. One should use a self-consistent model of the solar granulation and follow the evolution of a tiny magnetic patch. Two basic physical ingredients are mandatory, namely, the close thermal coupling with a cool environment and the existence of islands of high pressure in the intergranules. The current simulations of the CC lack of the first ingredient, which explains why they have not shown the effect that we advocate. All CC simulations begin with a tube in hydrostatic equilibrium with the temperature of the mean photosphere. The fluxtubes are already in the final state that the TRIP pursues which frustrates any additional concentration.

Having a fast and effective way of concentrating very weak magnetic fluxes results attractive. It may help understanding several observations whose interpretation is otherwise difficult. We will comment on some of them to illustrate the possibilities, acknowledging the speculative character of the connections.

- Recent observations have shown a reservoir of weak flux not yet concentrated magnetic features<sup>6</sup> (the work by Lin & Rimmele repeatedly mentioned along the paper). They form the natural starting materials for any concentration process, since regions of diluted fields and larger fluxes are not observed. Consequently, any pathway to generate the network magnetic elements necessarily needs of a first concentration of weak flux precursors (§1). This poses a problem to the CC since it cannot produce the observed 1.5 kG network field strengths. As mentioned above, the operation of the CC upon features of the reservoir (say, elements having a few times  $10^{16}$  Mx) yields field strengths of some 1 kG. The merging of many 1 kG features renders a 1 kG stable structure that cannot undergo a further concentration by CC (it is above the solid lines in Fig. 1). Such difficulty is automatically overcome by the TRIP that leads to 1.5 kG (§2).
- Quiet Sun magnetic concentrations suffer the continuous rattle of a dynamic environment, which stimulates the onset of instabilities. In particular, it excites interchange instabilities tending to split the structures into smaller pieces (see Schüssler 1986 and references therein). This process threaten the CC, since the tube sizes may become below the threshold where the required quasi-adiabatic evolution of the magnetized plasma is no longer easy. On the contrary, splitting into smaller fluxtubes facilitates the radiative cooling and therefore the operation of the TRIP.

---

<sup>6</sup>The turbulent fields diagnosed using Hanle effect techniques may also be included in this category; see Stenflo et al. (1998).

- The line polarization observed in the quiet Sun indicates a magnetic photosphere of very complex topology (Sánchez Almeida et al. 1996; Sigwarth et al. 1999; Sánchez Almeida & Lites 2000). This puzzling polarization can be generated by a collection of optically thin magnetic fluxtubes having dissimilar properties (Sánchez Almeida & Lites 2000). Such semi-empirical scenario gets strong support if the formation of most observed structures results from the gathering of many independent tiny sub-structures.

We do not want to finish without a clear statement on the complementarity between the CC and the TRIP. They complete each other rather than compete. Following convective motions, magnetic structures having a variety of magnetic field strengths and sizes reach the intergranular lanes. Then both mechanisms operate, the horizontal size of the structure being the factor that favors one or the other.

Thanks are due to an anonymous referee whose criticisms led to the development of some of the arguments in the paper. This work has been partly funded by the Spanish DGICYT under project 95-0028-C. It was carried out within the EC-TMR European Solar Magnetometry Network.

## A. Appendix A

Reaching kG fields at photospheric levels does not depend on the field strength existing in the deep sub-photosphere. A perturbation of the magnetic field at the bottom of the atmosphere  $\Delta B(z_0)$  induces a change of the photospheric field  $\Delta B(z)$ . The relationship between them is approximately given by

$$\Delta B(z)/B(z) \simeq \frac{\partial \ln B(z)}{\partial \ln B(z_0)} \Delta B(z_0)/B(z_0). \quad (\text{A1})$$

Using equation (7) to evaluate the derivative, one ends up with

$$\frac{\partial \ln B(z)}{\partial \ln B(z_0)} = \frac{\beta(z)}{\beta(z_0)}, \quad (\text{A2})$$

where  $\beta$  stands the familiar plasma beta,

$$\beta(z) = 8\pi P(z)/B(z)^2 = 1/[B(z)/B_m(z)]^2 - 1. \quad (\text{A3})$$

For a diluted field in the sub-photosphere (say,  $B[z_0]/B_m[z_0] \sim 0.1$ ) and the typical photospheric enhancement ( $B[z]/B_m[z] \sim 0.9$ ), equations (A2) and (A3) yield

$$\frac{\partial \ln B(z)}{\partial \ln B(z_0)} \simeq 2 \times 10^{-3}. \quad (\text{A4})$$

Equations (A1) and (A4) point out that  $B(z_0)$  has to vary by more than two orders of magnitude to produce a variation of the field strength in the observable layers. The dependence of  $B(z)$  on the temperature of the intergranules  $T$  can be evaluated in a similar way. It yields

$$\frac{\partial \ln B(z)}{\partial \ln T} \simeq -\beta(z)(z - z_0)/(2H) \sim -0.5. \quad (\text{A5})$$

The dependence on the temperature is much larger, although a 1200 K temperature variation modifies the field strength by only 10%.

## REFERENCES

- Baur, T. G., Elmore, D. E., Lee, R. H., Querfeld, C. W., & Rogers, S. R. 1981, *Sol. Phys.*, 70, 395
- Beckers, J. M., & Schöter, E. H. 1968, *Sol. Phys.*, 4, 142
- Berger, T. E., & Title, A. M. 1996, *ApJ*, 463, 365
- Bevington, P. R. 1969, *Data Reduction and Error Analysis for the Physical Sciences* (New York: McGraw-Hill)
- Cattaneo, F. 1999, *ApJ*, 515, L39
- Cox, J. P., & Giuli, R. T. 1968, *Principles of Stellar Structure* (New York: Gordon & Breach)
- Dunn, R. B., & Zirker, J. B. 1973, *Sol. Phys.*, 33, 281
- Giovanelli, R. G. 1977, *Sol. Phys.*, 52, 315
- Harvey, J. W., Livingston, W. C., & Slaughter, C. D. 1972, in *Line Formation in the Presence of Magnetic Fields*, ed. R. G. Athay, L. L. House, & G. A. Newkirk (Boulder: NCAR), 227
- Hasan, S. S. 1986, *A&A*, 143, 39
- Hassan, S. S., & van Ballegoijen, A. A. 1998, in *Cool Stars, Stellar Systems and the Sun: Tenth Cambridge Workshop*, ed. R. A. Donahue & J. A. Bookbinder, *ASP Conf. Ser.* 154 (San Francisco: ASP), CD 630
- Howard, R., & Stenflo, J. O. 1972, *Sol. Phys.*, 22, 402

- Khomenko, E., Collados, M., Bellot Rubio, L. R., Rodríguez Hidalgo, I., & Ruiz Cobo, B. 1999, in Proc. of the 9th European Meeting on Solar Physics: Magnetic Fields and Solar Processes, ed. A. Wilson, ESA SP Series 488, in press
- Kovitya, P., & Cram, L. 1983, Sol. Phys., 84, 45
- Lin, H. 1995, ApJ, 446, 421
- Lin, H., & Rimmele, T. 1999, ApJ, 514, 448
- Mehltretter, J. P. 1974, Sol. Phys., 38, 43
- Meyer, F., Schmidt, H. U., Simon, G. W., & Weiss, N. O. 1979, A&A, 79, 35
- Mihalas, D. 1967, in Methods in Computational Physics 7, ed. B. Alder, S. Fernbach, & M. Rotenberg (New York: Academic Press), 1
- Muller, R. 1985, Sol. Phys., 100, 237
- Muller, R. 1994, in Solar Surface Magnetism, ed. R. J. Rutten & C. J. Schrijver, NATO ASI Ser. 433 (Dordrecht: Kluwer), 55
- Parker, E. N. 1963, ApJS, 8, 177
- Parker, E. N. 1978, ApJ, 221, 368
- Parker, E. N. 1979, Cosmical Magnetic Fields (Oxford: Clarendon Press)
- Rajaguru, S., & Hasan, S. S. 1999, in High Resolution Solar Physics: Theory, Observations, and Techniques, ed. T. R. Rimmele, K. S. Balasubramaniam, & R. R. Radick, ASP Conf. Ser. 183 (San Francisco: ASP), 53
- Rüedi, I., Solanki, S. K., Livingston, W., & Stenflo, J. O. 1992, A&A, 263, 323
- Sánchez Almeida, J. 1997, ApJ, 491, 993
- Sánchez Almeida, J. 1998, in Three-Dimensional Structure of Solar Active Regions, ed. C. E. Alissandrakis & B. Schmieder, ASP Conf. Ser. 155 (San Francisco: ASP), 54
- Sánchez Almeida, J., Landi Degl’Innocenti, E., Martínez Pillet, V., & Lites, B. W. 1996, ApJ, 466, 537
- Sánchez Almeida, J., & Lites, B. W. 2000, ApJ, 532, 1215

- Schüssler, M. 1986, in *Small Scale Magnetic Flux Concentrations in the Solar Photosphere*, ed. W. Deinzer, M. Knölker, & H. H. Voigt (Göttingen: Vandenhoeck & Ruprecht), 103
- Seaton, M. J., Yan, Y., Mihalas, D., & Pradhan, A. K. 1994, *MNRAS*, 266, 805
- Sheeley, N. R. 1967, *Sol. Phys.*, 1, 171
- Sigwarth, M., Balasubramaniam, K. S., Knölker, M., & Schmidt, W. 1999, *A&A*, 349, 941
- Solanki, S. K., Zufferey, D., Lin, H., Rüedi, I., & Kuhn, J. R. 1996, *A&A*, 310, L33
- Spiegel, E. A. 1957, *ApJ*, 126, 202
- Spruit, H. C. 1979, *Sol. Phys.*, 61, 363
- Spruit, H. C. 1981, *A&A*, 98, 155
- Spruit, H. C. 1982, *Sol. Phys.*, 75, 3
- Stein, R. F., & Nordlund, Å. 1998, *ApJ*, 499, 914
- Stenflo, J. O. 1973, *Sol. Phys.*, 32, 41
- Stenflo, J. O., Harvey, J. W., Brault, J. W., & Solanki, S. K. 1984, *A&A*, 131, 333
- Stenflo, J. O., Keller, C. U., & Gandorfer, A. 1998, *A&A*, 329, 319
- Stix, M. 1991, *The Sun* (Berlin: Springer-Verlag)
- Takeuchi, A. 1999, *ApJ*, 522, 518
- van Ballegooijen, A. A. 1984, in *Small-Scale Dynamical Processes in Quiet Stellar Atmospheres*, ed. S. L. Keil, NSO/SP Workshops (Sunspot NM: NSO), 260
- van Ballegooijen, A. A., Nisenson, P., Noyes, R. W., Löfdahl, M. G., Stein, R. F., Nordlund, Å., & Krishnakumar, V. 1998, *ApJ*, 509, 435
- Venkatakrishnan, P. 1986, *Nature*, 322, 156
- Wiehr, E. 1978, *A&A*, 69, 279

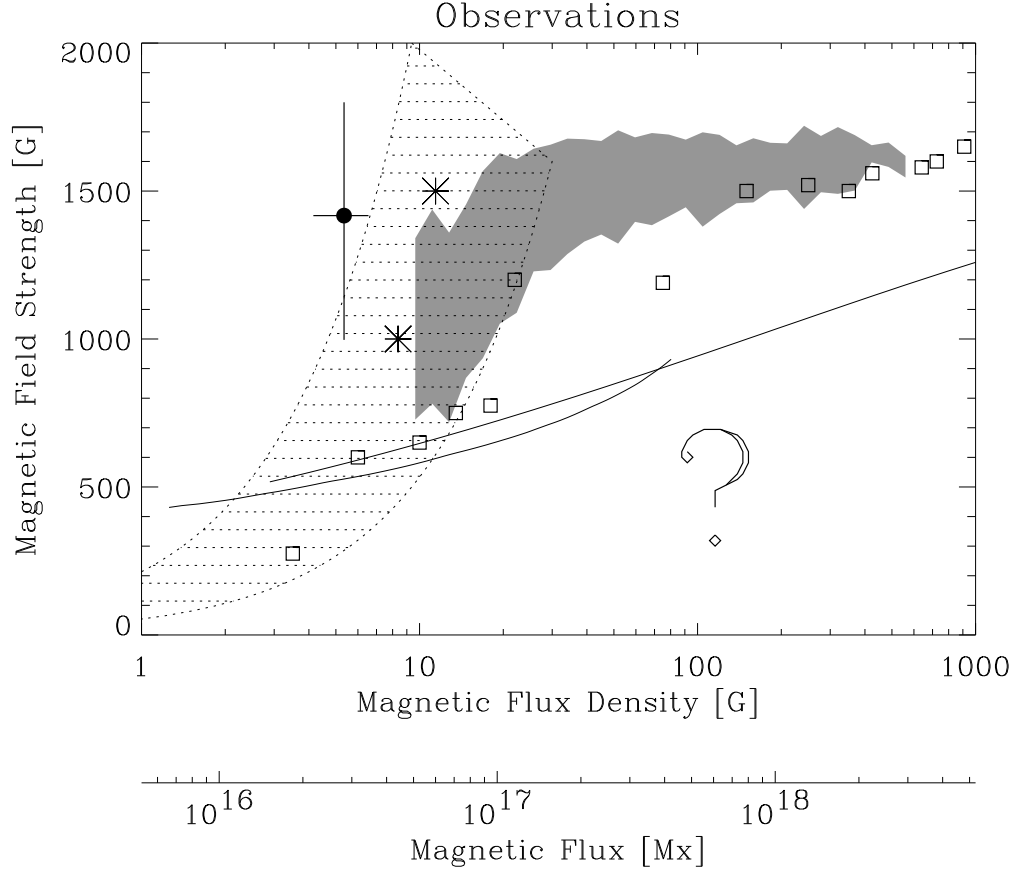


Fig. 1.— Observations of magnetic field strength versus magnetic flux density (i.e., the magnetic flux per unit resolution element). It summarizes the current status: the squares come from Solanki et al. (1996), the hashed region corresponds to the limits observed by Lin (1995) and Lin & Rimmele (1999), the shadowed region represents the mean  $\pm$  the standard deviation of the data in Sánchez Almeida & Lites (2000) and, finally, the two stars show structures which may be final stages of the Convective Collapse (CC; Lin & Rimmele 1999, and Khomenko et al. 1999). According to the CC mechanism, points below (above) the solid lines are unstable (stable) (these theoretical predictions were evaluated by Rajaguru & Hasan 1999, the low flux region, and by Takeuchi 1999, the high flux region). The CC moves points across this border following vertical trajectories (it occurs at a constant magnetic flux). Note that there are two regions devoid of observations; the one with the question mark is accessible to the present magnetometers so that it is really empty. The other one, corresponding to strong fields but weak fluxes, seems to be below sensitivity of present instrumentation. (The bullet with error bars represents an effort carried out in §4 to show that this region may be populated.) Magnetic flux densities have been transformed to magnetic flux (and vice versa) assuming an angular resolution of 1'' ( $1\text{G flux density} \equiv 1\text{G} \times (725\text{ km})^2 \simeq 5.3 \times 10^{15}\text{ Mx magnetic flux}$ ). Except for the IR data of Lin (1995) and Lin & Rimmele (1999), the magnetic field strengths are evaluated at the base of the photosphere, i.e., where the continuum optical depth of the unmagnetized Sun equals one and the pressure amounts to  $1.3 \times 10^5\text{ dyn cm}^{-2}$ .

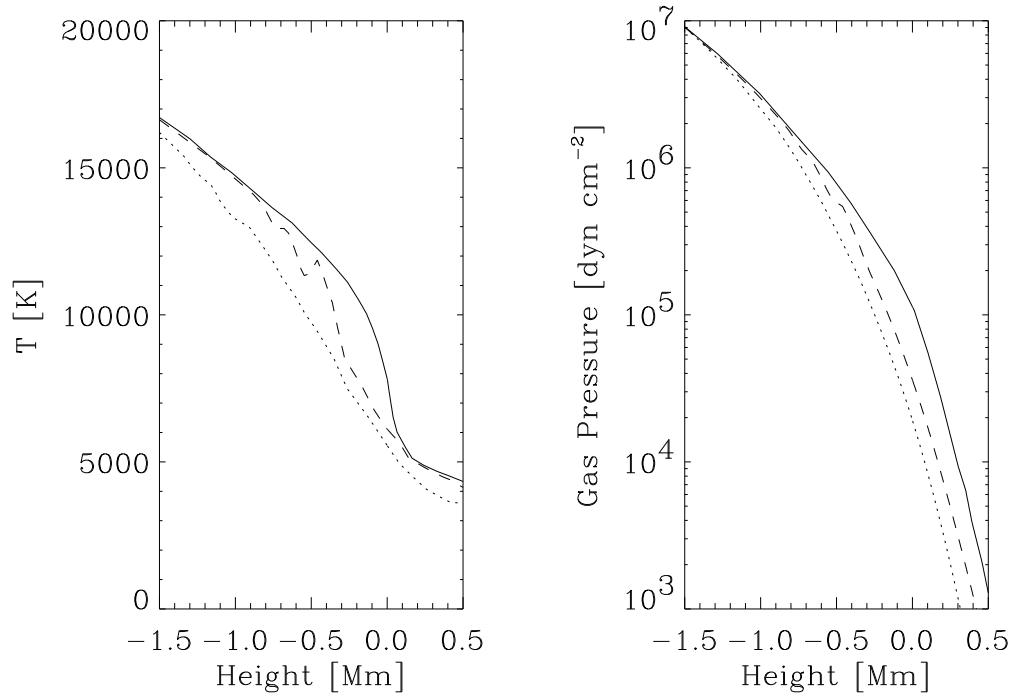


Fig. 2.— Temperature stratifications (left) and gas pressure stratifications (right) corresponding to realistic numerical simulations of the solar granulation (Stein & Nordlund 1998). The solid lines stand for the mean values whereas the dotted and dashed lines represent intergranules. The pressures of the intergranules that we show are not their real pressures, but the pressure if they were in hydrostatic equilibrium. The real intergranular pressures have to be of the order of the mean pressure (see main text). The reduction of hydrostatic equilibrium pressures with respect to the mean pressure is responsible for the concentration of the magnetic fields, whose strengths have to increase to balance this deficit. Heights are given in Mm from the layer where the continuum optical depth equals one.

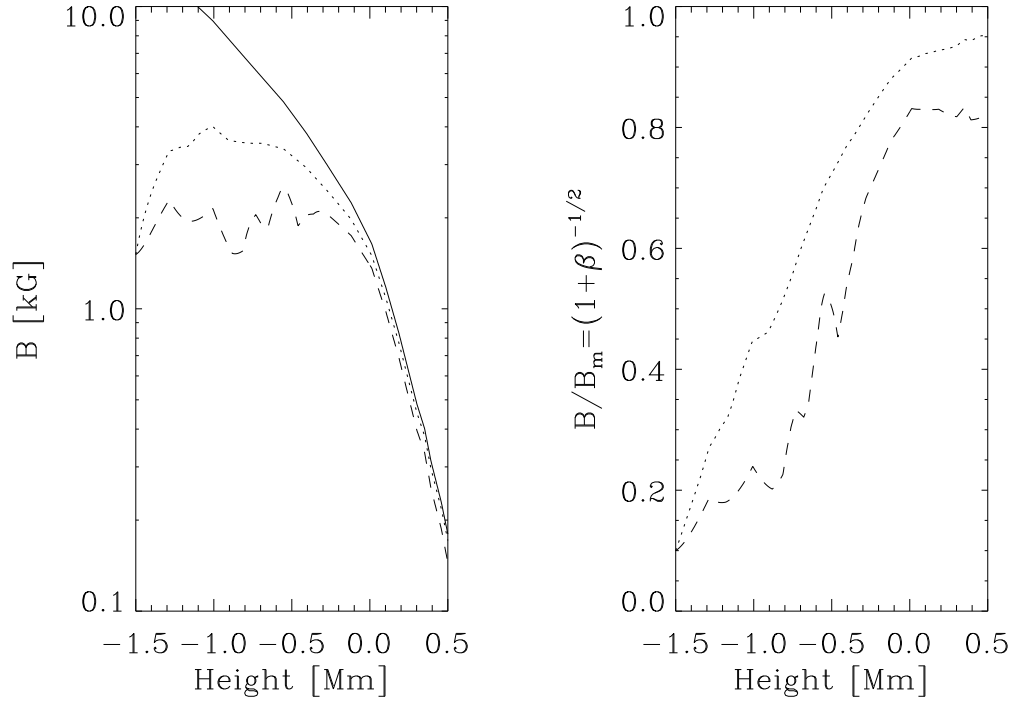


Fig. 3.— Left: variation with height in the atmosphere of the magnetic field strengths produced by the TRIP. The solid line is the maximum possible field strength  $B_m$ , which corresponds to a fully evacuated fluxtube. The dashed and dotted lines represent the magnetic fields to be found within the intergranules of Figure 2. Right: magnetic field strength referred to  $B_m$ . (The equivalence between this quantity and the plasma  $\beta$  is in the label of the plot.) In good agreement with observations,  $B/B_m \sim 0.9$  when  $z > 0$ . Heights are given in Mm from the layer where the continuum optical depth equals one ( $z = 0$ ).

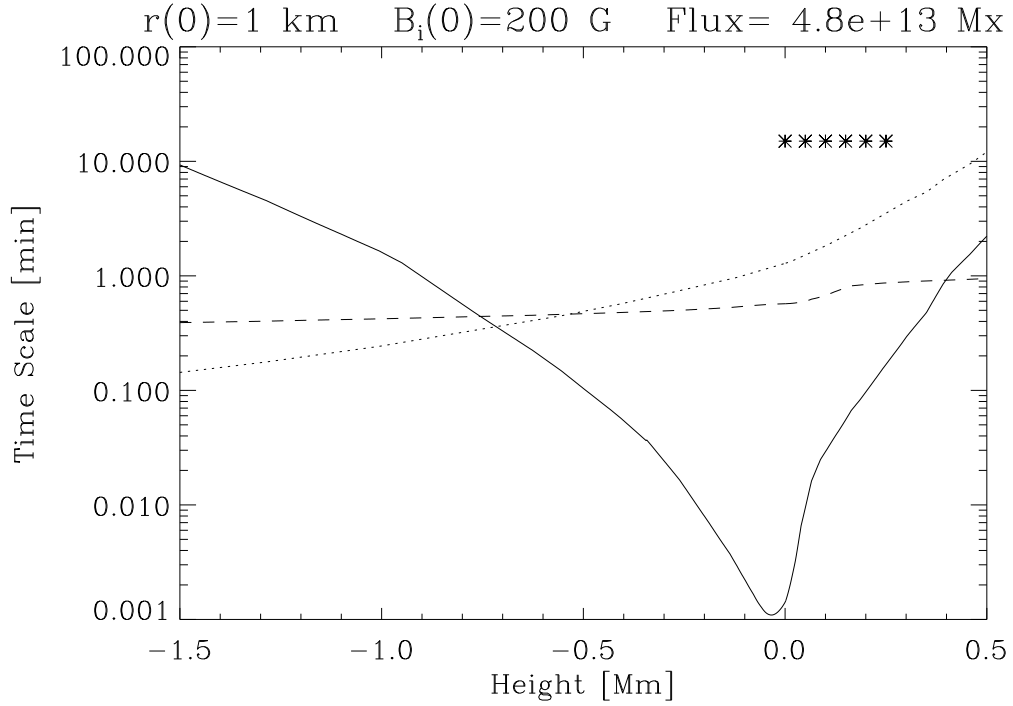


Fig. 4.— Time scales of the physical processes that lead a magnetic concentration to reach the properties set by its environment. The solid line shows the time to reach the temperature of the surroundings, whereas the dashed line corresponds to the time to set hydrostatic equilibrium along field lines. They are much shorter than the observed lifetimes of the quiet Sun magnetic structures, represented in the figure by the stars spanning 350 km above the photosphere. The dotted line corresponds to the time scale for ohmic diffusion, a process slower than the cooling of the structure. Keep in mind that the TRIP mainly involves layers 500 km below the base of the photosphere (i.e., heights between -0.5 Mm and 0.0 Mm).

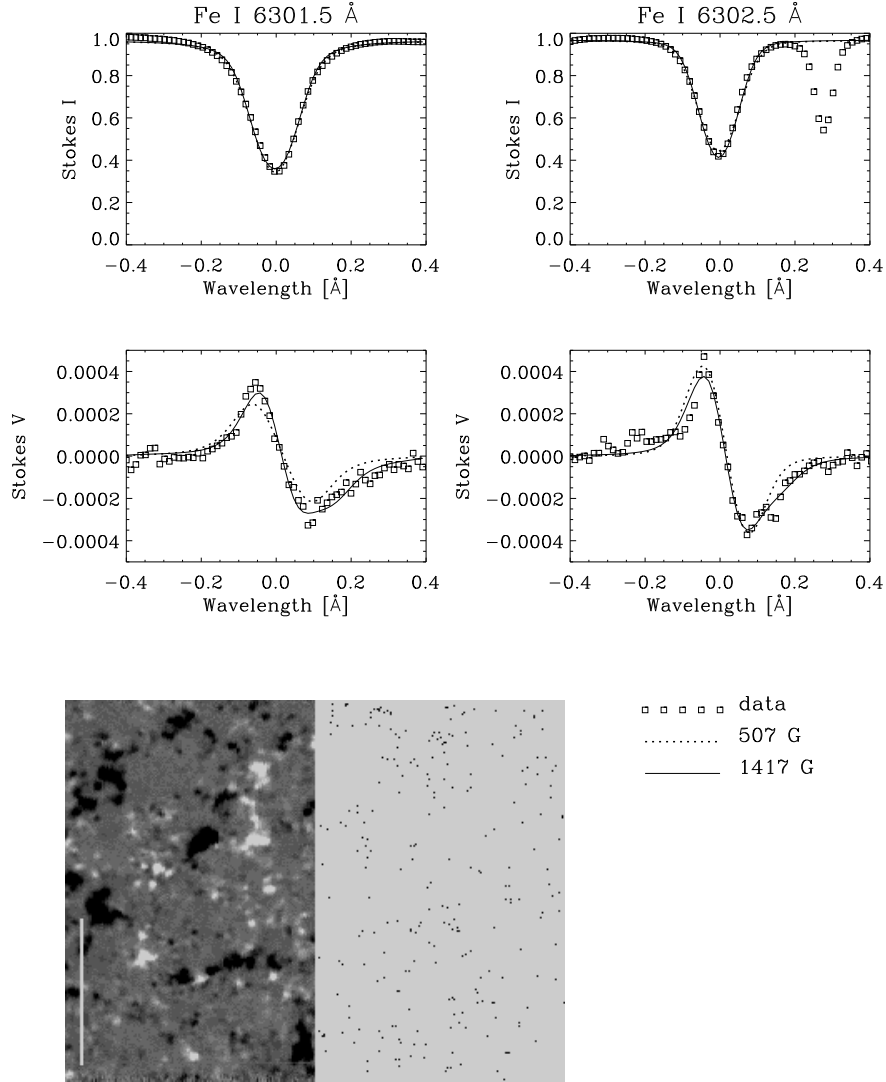


Fig. 5.— Composite plot showing the polarization profiles used to infer weak flux yet concentrated magnetic regions in the Sun (the point with error bars in Fig. 1). The intensity (Stokes  $I$ ) and the circular polarization (Stokes  $V$ ) of the lines Fe I  $\lambda$ 6301.5 and Fe I  $\lambda$ 6302.5 are represented versus the wavelength. The observations (squares) are best reproduced by a 1417 G field magnetic feature (the solid line) as compared to a structure having 500 G (the dotted lines). Note the extreme weakness of the signals (maximum degree of polarization about  $4 \times 10^{-4}$ ). The inset at the bottom contains a magnetogram of the solar region from which the data were extracted. It clearly shows the network and some internetwork fields (the vertical scale corresponds to 25 000 km on the solar surface). The image next to the magnetogram points out those pixels averaged to produce the observed Stokes profiles; note that there is no obvious correspondence with network points.